Munawwar Mohabuth, Aditya Khanna, James Hughes, James Vidler, Andrei Kotousov, Ching-Tai Ng

On the determination of the third-order elastic constants of homogeneous isotropic materials utilising Rayleigh waves

Ultrasonics, 2019; 96:96-103

Published at: http://dx.doi.org/10.1016/j.ultras.2019.02.006

On the determination of third-order elastic constants utilising Rayleigh waves

Munawwar Mohabuth[a,*], Aditya Khanna[a], James Hughes[a], James Vidler[a], Andrei Kotousov[a], Ching-Tai Ng[b]

[a]*School of Mechanical Engineering, The University of Adelaide, Adelaide, SA 5005, Australia*

[b]*School of Civil, Environmental and Mining Engineering, The University of Adelaide, Adelaide, SA 5005, Australia*

[*]Corresponding Author. E-mail address: munawwar.mohabuth@adelaide.edu.au

Abstract: This paper presents a new method for determining the third-order elastic constants (TOECs) of an isotropic material utilising the acoustoelastic effect associated with Rayleigh waves. It is demonstrated that the accuracy of the evaluation of TOECs can be substantially improved by supplementing the classical equations of acoustoelasticity, which describe the effect of applied stress on bulk wave speeds, with the nonlinear characteristic equation for the propagation of Rayleigh waves in pre-stressed media.

The developed method is applied to the experimental evaluation of the TOECs of an Aluminium alloy and the measured values are found to compare favourably with previously reported results obtained using bulk waves. The observed discrepancies can be explained by the anisotropy and non-homogeneity of the tested sample, specifically near the surface, which affect the Rayleigh wave propagation. The developed method can be readily implemented for Structural Health Monitoring applications; for example, the measurement of applied stresses based on the acoustoelastic effect, or the monitoring of near-surface damage based on the change in magnitude of the TOECs.

Keywords: Acoustoelasticity; Rayleigh waves; Material properties; Murnaghan constants; Stress measurement.

1. Introduction

In classical linear elasticity, the stress-strain response of an isotropic material is fully described by two second-order elastic constants. However, several experimentally observed phenomena, such as the variation of wave speeds with applied loading [1-4] or changes in compressibility with hydrostatic pressure [5-9], need consideration of the so-called third order elastic constants (TOECs). These constants arise in the expansion of the elastic strain energy density function and account for the contribution of the third-order products of the strain components. For an isotropic material, it can be shown that, in addition to the two second-order elastic constants, there are three independent third-order elastic constants corresponding to the third-order terms in the power series expansion of the strain energy density [10]. Various definitions of these constants were suggested by Brillouin [11], Biot [12,13], Landau & Lifshitz [14] and others [15-18].

TOECs play an important role in various engineering applications; for example, the evaluation of applied or residual stresses based on the acoustoelastic theory, which describes the propagation of small-amplitude waves in a material subjected to finite deformations [19,20]. Another important recent development exploits the much greater sensitivity of TOECs as compared with second-order elastic constants to dislocation driven damage (fatigue, creep, etc) [21-23]. This effect motivated the development of experimental techniques, such as second and higher harmonic generation to evaluate the so-called early damage [24-27], i.e. damage accumulated prior to the formation of a propagating crack. However, these experimental techniques often require highly accurate measurements of the TOECs to allow for quantitative damage identification.

TOECs are typically evaluated by measuring the change in bulk wave speeds with applied stress and fitting the measured values into the analytical equations of the acoustoelastic theory [28-30]. However, these measurements are still very challenging, and a large scatter is normally reported. A high frequency signal (toneburst) in the MHz range is normally employed in conjunction with a high sampling frequency of the data acquisition system to achieve a good temporal resolution in the wave speed measurements. However, the excitation frequency is restricted by certain natural limitations; for example, the wavelength (or the central frequency of the toneburst) is limited by the size of the surface asperities or the material texture, which can affect the measurements. However, it seems that spatial resolution has a greater effect on the accuracy of the evaluation of TOECs with bulk waves, specifically for slender structures, or small measurement gauge lengths. A significant improvement in the accuracy has been achieved with non-contact measurement techniques, such as laser interferometry. However, the reported values still have a large scatter; this might not be satisfactory for damage evaluation, especially in the case of fatigue damage, where the change in the TOECs are expected to be within 10 - 20% during the whole fatigue life.

An improvement in the evaluation of TOECs can be achieved using guided waves, which can propagate over large distances without significant attenuation. The advantage of using guided waves includes the possibility of an increased gauge length and hence, an expected improvement in the spatial resolution [31]. Another advantage is the possibility of utilising different types or modes of guided waves, which are known to be more sensitive to applied stresses as compared to bulk waves, specifically near the cut-off frequencies [32]. On the other hand, the main disadvantage of using guided waves is that it requires complex signal processing techniques due to the dependence of the guided wave speeds on the frequency (dispersion) and the excitation of multiple modes, which is inevitable in all guided wave excitation methods.

The present paper investigates the use of Rayleigh waves in conjunction with bulk waves for the evaluation of TOECs. Rayleigh waves are a type of non-dispersive guided waves that propagate near the surface of thick structures. The penetration depth of these surface waves depends on the excitation frequency; this phenomenon can potentially be utilised for tomography of damage or stress but this is beyond the scope of the current study. The structure of this paper is as follows. In the next section, the acoustoelastic theory and the governing equations for bulk waves and Rayleigh waves are reviewed. This set of analytical equations forms the theoretical foundation for different methods of evaluating the TOECs. The accuracy of these methods is investigated using Monte-Carlo simulations, taking into account various types of probabilistic distributions of the wave speed measurements. Further, an example of actual measurements, including the experimental set-up and signal processing methodology, is presented, followed by a discussion of the outcomes of the theoretical study as well as the experimental measurements. The main outcomes of this paper are briefly summarised in the conclusion.

2. Review of governing equations of acoustoelasticity

The governing equations of acoustoelasticity are briefly recapped here following Ogden et al. [33]. The equations for incremental motions due to the propagation of small-amplitude elastic waves as well as the incremental constitutive equation for a homogeneously deformed medium, can be written as:

$$\mathcal{A}_{piqj}\,\frac{\partial^2 u_j}{\partial x_p \partial x_q} = \rho\,\frac{\partial^2 u_i}{\partial t^2}\,, \tag{1}$$

and

$$\hat{S}_{pi} = \mathcal{A}_{piqj}\,\frac{\partial u_j}{\partial x_q}, \tag{2}$$

respectively, where $\boldsymbol{\mathcal{A}}$ is the fourth-order tensor of instantaneous elastic moduli, ρ is the density of the material in the deformed configuration, $\boldsymbol{u}$ is the incremental displacement vector associated with the wave, $\boldsymbol{x}$ is the position vector in the deformed configuration, t is the time and $\widehat{\boldsymbol{S}}$ is the incremental nominal stress tensor. The reader is referred to [34] for the derivation of the above equations.

The strain energy function commonly used to evaluate the acoustoelastic effect in engineering materials subjected to a small pre-stress is due to Murnaghan [15] and is given by

$$W = \frac{1}{2}(\lambda + 2\mu)i_1^2 - 2\mu i_2 + \frac{1}{3}(l + 2m)i_1^3 - 2m\, i_1 i_2 + n i_3, \tag{3}$$

where i_1, i_2, i_3 are the principal invariants of the Green-Lagrange strain tensor $\boldsymbol{E}$, given by $i_1 = \mathrm{tr}\boldsymbol{E}$, $i_2 = \frac{1}{2}[i_1^2 - \mathrm{tr}(\boldsymbol{E})^2]$ and $i_3 = \det \boldsymbol{E}$, respectively. The parameters λ and μ are the classical Lamé elastic constants and l, m, n are the Murnaghan or third-order elastic constants. Using the above strain energy function, the elasticity tensor can be obtained to the first order in the strain as [35]

$$\begin{aligned} J\mathcal{A}_{piqj} = {} & \mu\left(\delta_{ij}\delta_{pq} + \delta_{iq}\delta_{jp}\right) + \lambda\delta_{ip}\delta_{jq} \\ & + 2\mu\left(2\delta_{ij}E_{pq} + \delta_{pq}E_{ij} + \delta_{iq}E_{jp} + \delta_{jp}E_{iq}\right) \\ & + \lambda\left(E\delta_{ij}\delta_{pq} + 2\delta_{ip}E_{jq} + 2\delta_{jq}E_{ip}\right) + 2lE\delta_{ip}\delta_{jq} \\ & + m\left[E\left(\delta_{ij}\delta_{pq} + \delta_{iq}\delta_{jp} - 2\delta_{ip}\delta_{jq}\right) + 2\left(\delta_{ip}E_{jq} + \delta_{jq}E_{ip}\right)\right] \\ & + \frac{1}{2}n\left[\delta_{ij}E_{pq} + \delta_{pq}E_{ij} + \delta_{iq}E_{jp} + \delta_{jp}E_{iq} - 2\delta_{ip}E_{jq} - 2\delta_{jq}E_{ip}\right. \\ & \left. - E\left(\delta_{ij}\delta_{pq} + \delta_{iq}\delta_{jp} - 2\delta_{ip}\delta_{jq}\right)\right], \end{aligned} \tag{4}$$

where $E = \mathrm{tr}\boldsymbol{E}$ and $J = 1 + E$.

For the experimental determination of TOECs, the test specimen is generally subjected to a static uniaxial stress state due to the simplicity of the loading apparatus. For a small applied uniaxial stress σ_{11} in the $\boldsymbol{e_1}$ direction, the components of the strain tensor $\boldsymbol{E}$ can be evaluated using the linear elasticity theory as follows:

$$E_{11} = \frac{\lambda + \mu}{3K\mu}\sigma_{11}, \quad E_{22} = E_{33} = -\frac{\lambda E_{11}}{2(\lambda + \mu)}, \tag{5}$$

where $K = \lambda + 2\mu/3$ is the bulk modulus. The expression for the Jacobian of the deformation then reduces to

$$J = 1 + \frac{\mu E_{11}}{\lambda + \mu} = 1 + \frac{\sigma_{11}}{3K}. \tag{6}$$

2.1. Bulk waves

Hughes and Kelly [1] first obtained the expressions for the stress-dependent speeds of bulk waves propagating along the principal directions, i.e. along the direction $\boldsymbol{e_1}$ of the uniaxial stress, and along the mutually perpendicular directions, $\boldsymbol{e_2}$ and $\boldsymbol{e_3}$, which are equivalent by symmetry. Following Abiza et al. [36] and Hughes and Kelly [1], the expressions for the speed of these principal waves can be written in terms of the components of the elasticity tensor $\boldsymbol{\mathcal{A}}$ as follows:

$$\rho_0 v_{11}^2 = J\mathcal{A}_{1111} = \lambda + 2\mu + \frac{\sigma_{11}}{3K}\left[2l + \lambda + \frac{\lambda + \mu}{\mu}(4m + 4\lambda + 10\mu)\right], \tag{7}$$

$$\rho_0 v_{12}^2 = J\mathcal{A}_{1212} = \mu + \frac{\sigma_{11}}{3K}\left[m + \frac{\lambda}{4\mu}n + 4\lambda + 4\mu\right], \tag{8}$$

$$\rho_0 v_{22}^2 = J\mathcal{A}_{2222} = \lambda + 2\mu + \frac{\sigma_{11}}{3K}\left[2l - \frac{2\lambda}{\mu}(m + \lambda + 2\mu)\right], \tag{9}$$

$$\rho_0 v_{21}^2 = J\mathcal{A}_{2121} = \mu + \frac{\sigma_{11}}{3K}\left[m + \frac{\lambda}{4\mu}n + \lambda + 2\mu\right], \tag{10}$$

$$\rho_0 v_{23}^2 = J\mathcal{A}_{2323} = \mu + \frac{\sigma_{11}}{3K}\left[m - \frac{\lambda + \mu}{2\mu}n - 2\lambda\right]. \tag{11}$$

where $\rho_0 = \rho J$ is the density of the material in the undeformed or unstressed configuration, and the applied uniaxial stress σ_{11} is positive in tension. The elastic moduli $\mathcal{A}_{piqj}$ can be evaluated by substituting Eq. (5) into Eq. (4). The speeds v_{11} and v_{12} in Eqs. (7) and (8) correspond to longitudinal and transverse waves respectively, propagating along the direction $\boldsymbol{e_1}$ of the applied uniaxial stress. In Eq. (9), v_{22} is the speed of the longitudinal wave propagating along the direction $\boldsymbol{e_2}$, which is perpendicular to the applied uniaxial stress. In Eqs. (10) and (11), v_{21} and v_{23} correspond to the speeds of transverse waves propagating along the direction $\boldsymbol{e_2}$ and polarised in the directions $\boldsymbol{e_1}$ and $\boldsymbol{e_3}$, respectively.

2.2.Rayleigh-Lamb waves

Mohabuth et al. [32] obtained the characteristic equations describing the acoustoelastic effect for plane Lamb wave propagation in pre-stressed plates along the principal direction of the applied uniaxial stress. The main steps in the derivation of these characteristic equations are provided in Appendix A. By considering the limit of the plate-thickness tending to infinity, the characteristic equations for Lamb wave propagation can be reduced to the equation governing the acoustoelastic effect for Rayleigh waves. This special case was first investigated by Dowaikh and Ogden [37] and the form of their original equation can be recovered by substituting Eqs. (A8) and (A10) into Eq. (A9), replacing c by c_R and recalling that $\rho = \rho_0 J^{-1}$, as follows:

$$(J\mathcal{A}_{1111} - \rho_0 c_R^2)(J\mathcal{A}_{1212} - \rho_0 c_R^2 - J\mathcal{A}_{2121})$$

$$+ \left(\frac{(J\mathcal{A}_{1111} - \rho_0 c_R^2)(J\mathcal{A}_{1212} - \rho_0 c_R^2)}{(J\mathcal{A}_{2222})(J\mathcal{A}_{2121})}\right)^{\frac{1}{2}} \{J\mathcal{A}_{2222}(J\mathcal{A}_{1111} - \rho_0 c_R^2) \tag{12}$$

$$- (J\mathcal{A}_{1122})^2\} = 0.$$

The stress-dependent elastic moduli $J\mathcal{A}_{1111}, J\mathcal{A}_{1212}, J\mathcal{A}_{2222}$ and $J\mathcal{A}_{2121}$ in the above equation have been defined previously in Eqs. (7)-(10). The remaining elastic modulus $J\mathcal{A}_{1122}$ can be obtained from Eq. (4) as

$$J\mathcal{A}_{1122} = \lambda + \frac{\sigma_{11}}{6K\mu}[4\mu l + 2\lambda m - \lambda n + 2\lambda(\lambda + 2\mu)]. \tag{13}$$

The characteristic Eq. (12) governing the acoustoelastic effect for Rayleigh waves differs from Eqs. (7)-(11) for bulk waves in two important respects. Firstly, the governing equation for Rayleigh waves contains all three TOECs, whereas the equations for bulk waves contain only two out of the three constants. Secondly, the characteristic Eq. (12) for Rayleigh waves contains the TOECs raised to exponents as well as terms involving products of the three TOECs. In principle, this implies that by substituting measured values of the Rayleigh wave speed at three known stress levels into Eq. (12), a system of three nonlinear equations can be obtained, from which all three TOECs can be determined.

3. Comparison of different methods for the determination of TOECs

Eqs. (7)-(11) provide a system of five linear equations in three unknown variables, l, m, and n for known values of the density ρ_0, Lamé constants, λ and μ, as well as the experimentally determined values of the bulk wave speeds at a known stress level, σ_{11}. The unknown TOECs can be determined by solving a system of any three out of five linear equations given by Eqs. (7)-(11). The system of Eqs. (9)-(11) is preferred over other combinations since the

experimental setup for the measurement of bulk wave speeds perpendicular the direction of the applied stress is relatively straightforward. As shown in Fig. 1, ultrasonic transducers can be placed directly on the lateral surfaces of the specimen and the time of propagation of the bulk wave across the specimen thickness can be measured by either using the pulse-echo or pitch-catch arrangement of the transducers.

Experimental studies utilising this traditional method have reported a large scatter in the obtained values of the constant l, relative to the constants m and n, despite careful measurements of the bulk wave speeds. Some of these reported values for Aluminium alloys are summarised in Table 1. The possibility of reducing the standard deviation in the values of the TOECs is investigated by considering an alternative system of equations comprising the characteristic Eq. (12) for Rayleigh waves and any two out of the three Eqs. (9)-(11). Rayleigh waves can be generated along the direction of the applied uniaxial stress by utilising a wedge-transducer, as shown in Fig. 1.

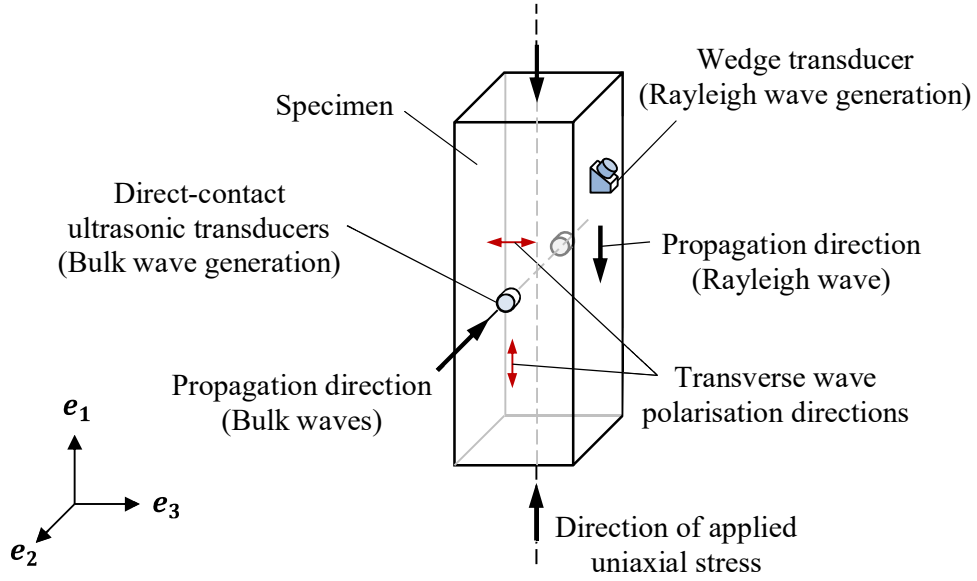

Fig. 1: Schematic diagram showing the propagation directions of the elastic waves and the direction of applied stress.

Table 1: Experimentally determined TOECs for Aluminium alloys reported by Smith et al. [29]

Aluminium alloys	Third order elastic constants (GPa)		
	l	m	n
2S	-311 ± 131	-401 ± 78	-408 ± 34
B53S M	-223 ± 61	-237 ± 12	-276 ± 5
B53S P	-201 ± 22	-305 ± 17	-300 ± 6
D54S	-387 ± 10	-358 ± 10	-320 ± 3
JH77S	-337 ± 32	-395 ± 13	-436 ± 7

The TOECs can be evaluated from the measurements of three wave speeds using any three out of four Eqs. (9)-(12). In this section, a comparative evaluation of the four possible combinations of these equations is conducted to identify the best combination which yields the smallest overall standard deviation in the obtained values of the TOECs. A numerical sensitivity study is conducted based on the various input parameters listed in Table 2. Based on the theoretical values of the Lamé constants, density and TOECs, the theoretical speeds of the three bulk waves, v_{22}, v_{21} and v_{23} and the Rayleigh wave, c_R, are evaluated at the stress level, σ_{11} using Eqs. (9)-(12). Following that, four datasets of 500 random speed measurements are generated with the following statistical distributions: (1) normal distribution with a standard deviation of 1 m/s (Fig. 2); (2) normal distribution with a standard deviation of 10 m/s; (3) uniform distribution over the interval defined by the theoretical speed ± 1 m/s; and (4) uniform distribution over the interval defined by the theoretical speed ± 10 m/s. For all four distributions, the mean values are set equal to the theoretical speeds obtained from Eqs. (9)-(12). For each of the four statistical distributions, the TOECs are evaluated for 500^3 = 125 million combinations of three wave speeds.

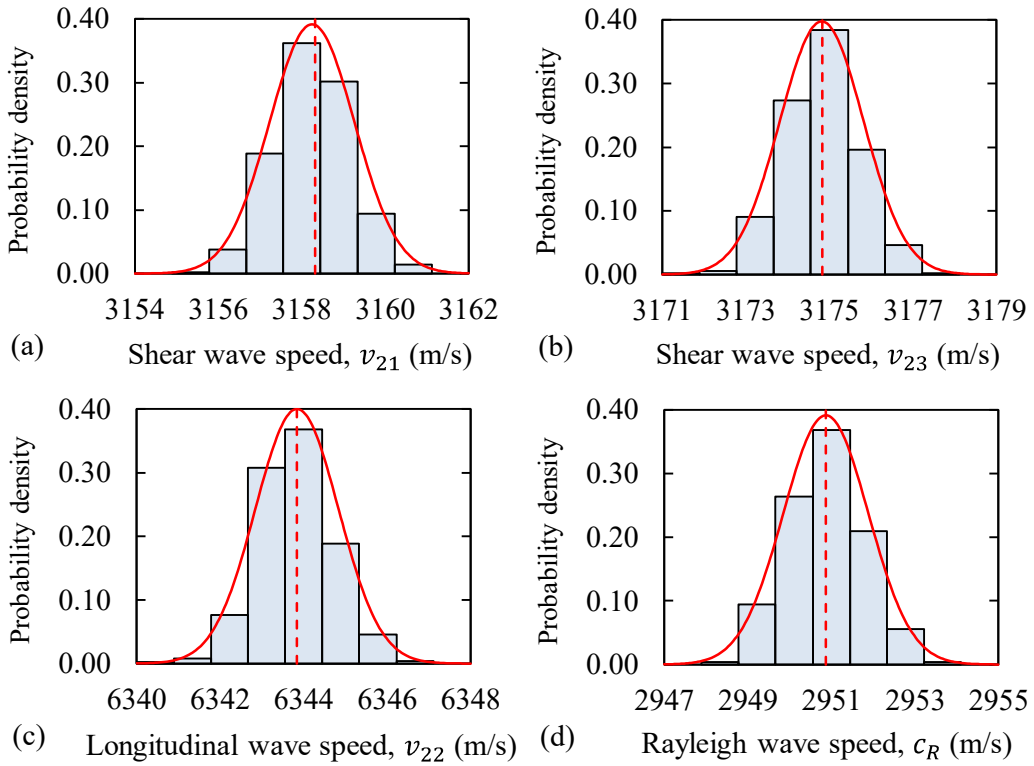

Fig. 2: Normal distribution of bulk and Rayleigh wave speeds with a standard deviation of 1 m/s. The sample means are equal to the theoretical wave speeds calculated using the input parameters listed in Table 2.

Table 2: Input parameters for the sensitivity study

Parameter	Value
λ (GPa)	54.308
μ (GPa)	27.174
l (GPa)	-281.5
m (GPa)	-339.0
n (GPa)	-416.0
ρ_0 (kg/m^3)	2704
σ_{11} (MPa)	100

The results of the sensitivity study are summarised in Tables 3-5. In these tables, the numerical values of the TOECs obtained using the four combinations of Eqs. (9)-(12) are presented for the various statistical distributions of wave speeds described previously. It can be observed that the mean values of the TOECs presented in Tables 3-5 are within a few percent of the exact values listed in Table 2, regardless of the choice of the statistical distribution or the system of equations used. This is in accordance with the law of large numbers, which states that the sample mean converges to the expected value as the number of repeat measurements tends to infinity. However, the standard deviation in the numerical values of all three constants is strongly linked to the scatter in the randomly generated wave speed distributions.

The best combination of three out of four Eqs. (9)-(12) can be identified by comparing the standard deviations in the numerically-evaluated values of the TOECs, presented in Tables 3-5. It is evident from the observation of Table 3 as well as Fig. 3 that the standard deviation in the numerical values of the constant l can be reduced substantially by utilising the characteristic Eq. (12) for Rayleigh waves in conjunction with any two out of three Eqs. (9)-(11), i.e. by utilising one of the proposed methods 2-4 rather than the traditionally utilised method 1. The standard deviation in the numerical values of the remaining constants, m and n is relatively insensitive to the choice of the method of solution, i.e. the combination of Eqs. (9)-(12) used. Overall, method 2 appears to be most suitable for the evaluation of the TOECs since it minimises the standard deviation for the constants l and n, while providing marginally greater standard deviation for the constant m, when compared to other methods.

Table 3: Comparison of the exact value of l = -281.5 GPa against numerical values obtained using the four combinations of wave speed measurements.

Wave speed distribution about theoretical value	Numerical value of l (mean ± std. dev.) in GPa			
	Method 1 v_{22}, v_{21}, v_{23}	Method 2 v_{22}, v_{21}, c_R	Method 3 v_{22}, v_{23}, c_R	Method 4 v_{21}, v_{23}, c_R
Normal distribution (std. dev. = 1 m/s)	-278.9 ± 67.8	-281.3 ± 17.5	-281.0 ± 26.8	-281.0 ± 26.0
Normal distribution (std. dev. = 10 m/s)	-282 ± 280	-282.0 ± 23	-282 ± 37	-282 ± 30
Uniform distribution (Resolution = 1 m/s)	-284.5 ± 39.3	-280.6 ± 16.2	-281.0 ± 21.8	-281.0 ± 24.8
Uniform distribution (Resolution = 10 m/s)	-282 ± 280	-282 ± 23	-282 ± 30	-282 ± 30

Table 4: Comparison of the exact value of m = -339 GPa against numerical values obtained using the four combinations of wave speed measurements.

Wave speed distribution about theoretical value	Numerical value of m (mean ± std. dev.) in GPa			
	Method 1 v_{22}, v_{21}, v_{23}	Method 2 v_{22}, v_{21}, c_R	Method 3 v_{22}, v_{23}, c_R	Method 4 v_{21}, v_{23}, c_R
Normal distribution (std. dev. = 1 m/s)	-338.1 ± 28.5	-338.4 ± 34.2	-337.3 ± 36.2	-338.8 ± 29.6
Normal distribution (std. dev. = 10 m/s)	-341 ± 164	-340 ± 269	-333 ± 275	-331 ± 274
Uniform distribution (Resolution = 1 m/s)	-340.3 ± 16.5	-337.7 ± 21.9	-338.7 ± 16.4	-339.0 ± 16.9
Uniform distribution (Resolution = 10 m/s)	-340 ± 164	-340 ± 269	-333 ± 275	-331 ± 274

Table 5: Comparison of the exact value of n = -416 GPa against numerical values obtained using the four combinations of wave speed measurements.

Wave speed distribution about theoretical value	Numerical value of n (mean ± std. dev.) in GPa			
	Method 1 v_{22}, v_{21}, v_{23}	Method 2 v_{22}, v_{21}, c_R	Method 3 v_{22}, v_{23}, c_R	Method 4 v_{21}, v_{23}, c_R
Normal distribution (std. dev. = 1 m/s)	-414.7 ± 25.9	-416.4 ± 14.3	-414.7 ± 32.0	-416.0 ± 12.6
Normal distribution (std. dev. = 10 m/s)	-417 ± 210	-415 ± 105	-412 ± 117	-412 ± 113
Uniform distribution (Resolution = 1 m/s)	-416 ± 15.1	-416.1 ± 12.9	-415.7 ± 12.6	-416.1 ± 7.5
Uniform distribution (Resolution = 10 m/s)	-409 ± 147	-416 ± 64.3	-409 ± 77	-419 ± 71

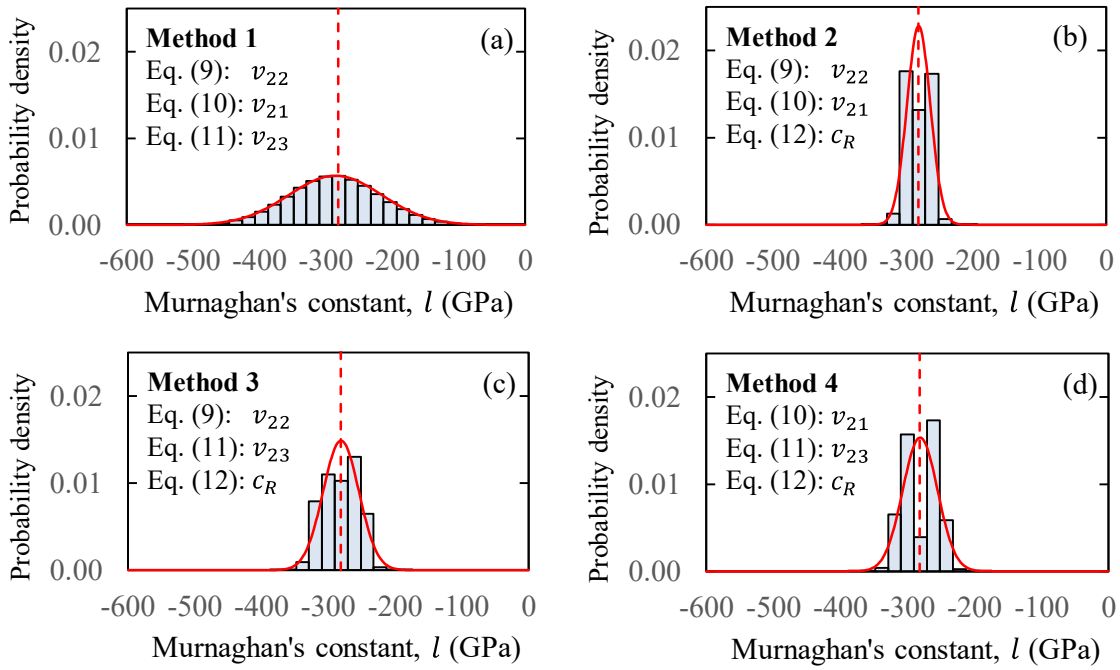

Fig. 3: The distribution of numerical values of the constant l obtained for the wave speed distributions shown in Fig. 2.

4. Linearisation of the governing equations of acoustoelasticity

One of the inherent shortcomings in the evaluation of TOECs based on wave speed measurements is the propagation of errors during the calculations. As demonstrated in the previous section, one way to improve the robustness of the calculations is to perform a large number of repeat measurements at a single stress level. Alternatively, one can take advantage of the approximately linear dependence of the wave speed on the applied stress within the elastic region of the stress-strain curve, i.e. for $\sigma_{11} \ll \lambda, \mu$. Rather than making several repeat measurements at a single stress level, the wave speed can also be measured at several increments of the applied stress. The slope of the wave speed vs. applied stress plot can then be evaluated using the method of least squares and the TOECs can be obtained from the linearised form of Eqs. (9)-(11). The linearised equations can be expressed solely in terms of the experimentally determined slope, $\partial v_{2k}/\partial \sigma_{11}$, $k \in [1, 2, 3]$, and the known material constants, λ, μ and ρ_0, as follows:

$$2\rho_0 v_{22,0} \frac{\partial v_{22}}{\partial \sigma_{11}} = \frac{1}{3K}\left[2l - \frac{2\lambda}{\mu}(m + \lambda + 2\mu)\right], \tag{14}$$

$$002\rho_0 v_{21,0} \frac{\partial v_{21}}{\partial \sigma_{11}} = \frac{1}{3K}\left[m + \frac{\lambda}{4\mu}n + \lambda + 2\mu\right], \tag{15}$$

$$2\rho_0 v_{23,0} \frac{\partial v_{23}}{\partial \sigma_{11}} = \frac{1}{3K}\left[m - \frac{\lambda + \mu}{2\mu}n - 2\lambda\right]. \tag{16}$$

In the above equations, the bulk wave speeds in the unstressed configuration are $v_{22,0} = \sqrt{(\lambda + 2\mu)/\rho_0}$ and $v_{21,0} = v_{23,0} = \sqrt{\mu/\rho_0}$. The nonlinear governing equation (12) for Rayleigh waves can also be linearised and written in terms of the experimentally determined slope $\partial c_R/\partial \sigma_{11}$. The resulting equation is quite lengthy and is presented in Appendix B. The correctness of the linearised Eqs. (14)-(16), (B1) can be verified by attempting to recalculate

the known values of TOECs listed in Table 2 based on theoretical obtained slopes $\partial v_{2k}/\partial\sigma_{11}$, $k \in [1,2,3]$ and $\partial c_R/\partial\sigma_{11}$.

Table 6: Comparison of known and calculated values of TOECs obtained from linearised equations

TOEC	Exact value	Method 1 v_{22}, v_{21}, v_{23}	Method 2 v_{22}, v_{21}, c_R	Method 3 v_{22}, v_{23}, c_R	Method 4 v_{21}, v_{23}, c_R
l (GPa)	-281.5	-281.5	-274.2	-286.3	-204.3
m (GPa)	-339.0	-339.0	-335.4	-341.4	-339.0
n (GPa)	-416.0	- 416.0	-423.3	-417.6	-416.0

The obtained values of the TOECs using various combinations of linearised equations are presented in Table 6. As expected, the system of linear equations (14)-(16) exactly recovers the known values of the TOECs. Methods 2 and 3, which utilise Eq. (14) and Eq. (B1) along with either Eq. (15) or Eq. (16) provide approximate values for the TOECs within 2.5%. This indicates a small error associated with the linearisation of the nonlinear Eq. (12). Method 4, which utilises Eqs. (15),(16) and (B1) must be avoided for the experimental evaluation of the TOECs since it yields a large error of roughly 27% in the value of the constant l.

5. Experimental measurement of TOECs

5.1. Experimental setup

The bulk wave speeds were measured in an Aluminium specimen with dimensions 416.5×183.5mm×47.6mm, and density 2741 kg/m^3. The Lamé constants were evaluated using bulk wave speed measurements in the unstressed specimen as $\lambda = 54.01$GPa and $\mu = 26.36$GPa. Measurements of the bulk wave speeds were achieved by using a pair of identical transducers on opposite sides of the specimen in a pitch-catch arrangement, as shown in Fig. 4. A pair of Olympus X1055 transducers were used for the excitation and sensing of longitudinal waves at a central frequency of 2.25 MHz. The longitudinal wave transducers were

coupled to the surface of the specimen using ISO68 hydraulic oil. A pair of Olympus V153-RM transducers were used for the excitation and sensing of transverse waves at a central frequency of 1 MHz. The transverse wave transducers were coupled to the surface of the specimen using a shear couplant with a high viscosity. The direction of polarisation of the transverse waves was controlled using an alignment fixture shown in Fig. 4. The excitation frequencies of the longitudinal and transverse waves were selected to match the central frequencies of the available transducers but different excitation frequencies may equivalently be used.

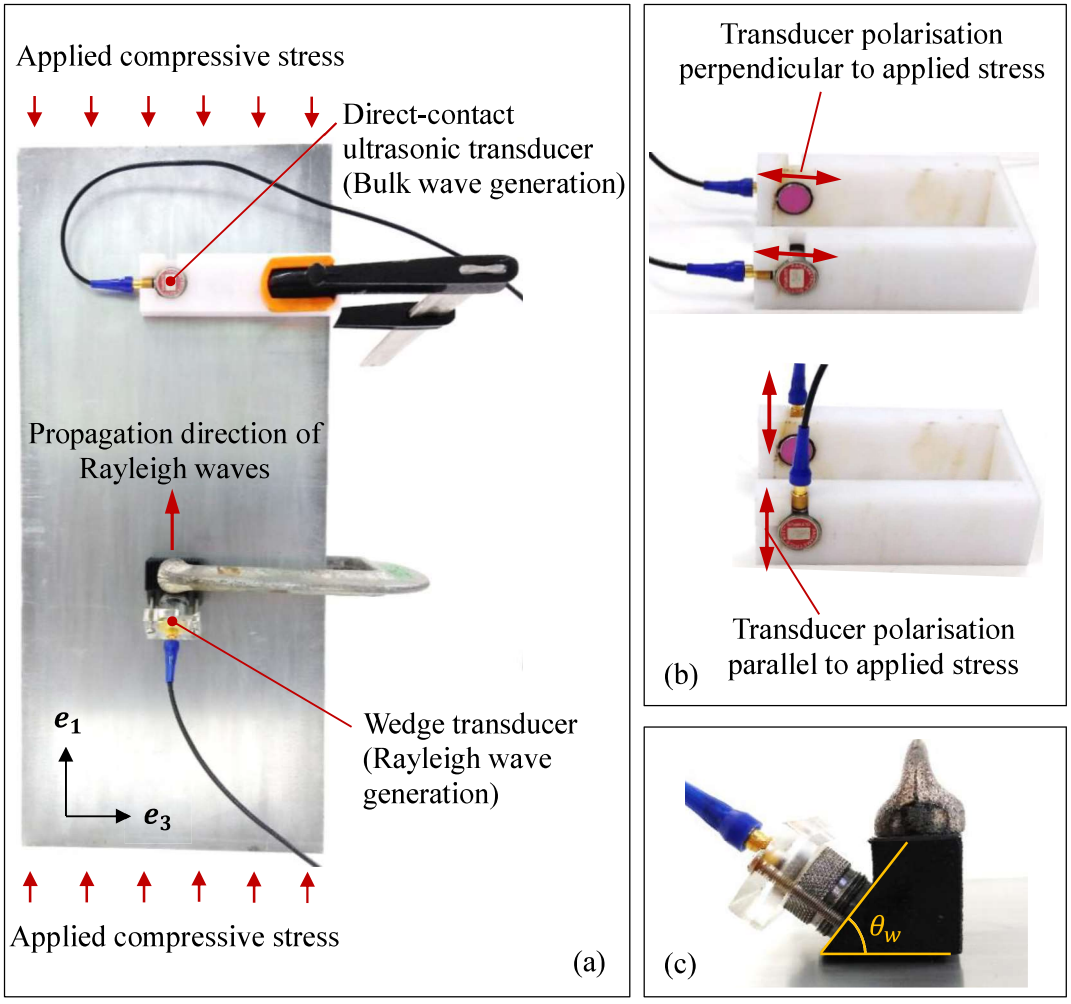

Fig. 4: (a) Experimental setup, (b) alignment fixture for generation and measurement of transverse waves, (c) wedge transducer for generation of Rayleigh waves.

The excitation toneburst signal was generated using a Tektronix AFG 3021B arbitrary function generator and amplified by 40 dB using a RITEC GA-2500A gated amplifier. A data acquisition system with a sampling rate of 102.4MHz was used, giving a temporal resolution of approximately 10ns. The signal was averaged 1000 times and a band pass filter was implemented between 500kHz and 20MHz to increase the signal-to-noise ratio. The changes in bulk wave speeds were recorded at 19 evenly-spaced increments of compressive uniaxial stress in the range 0MPa to 104.7MPa. The measurements were repeated five times at each load level to evaluate the consistency. Two strain gauges were bonded to the specimen to measure the axial and lateral strains corresponding to the applied uniaxial compressive stress. The lateral strain measurement was used to determine the change in the thickness of the specimen during loading, i.e. the change in the propagation distance of the bulk waves. The Rayleigh wave speed measurements for the same specimen were obtained from Hughes et al. [38] and the experimental setup and signal processing approach are described in the latter publication.

5.2. Signal processing

Fig. 5 (a)-(c) show the typical time domain signals for the three principal bulk waves travelling perpendicular to the applied stress. All the recorded signals show the arrival of the primary wave followed by multiple echoes, resulting from the reflection of the wave between the parallel surfaces of the specimen. A small wave packet can be identified prior to the arrival of the primary wave, which is a result of electromagnetic interference or cross-talk. The time of flight is evaluated using the cross-correlation method. The measured values of the change in bulk wave speeds with stress increment are shown in Fig. 5 (d)-(f). The observed trends are consistent with the theoretical predictions of Eqs. (14)-(16). The slopes of the lines of best fit as well as the upper and lower 95% confidence intervals for Fig. 5 (d)-(f) are recorded in Table

7. The corresponding values for Rayleigh waves are obtained from the analysis of the experimental data collected by Hughes et al. [38]. These are also included in Table 7.

The observed scatter in the measurement of the longitudinal wave speed is found to be much greater than the scatter observed in the measurement of transverse wave speeds. The larger scatter can be attributed to two main reasons: (1) the time of flight of the longitudinal waves is approximately half of the time of flight of the transverse waves, thereby increasing the relative error in the measurements, and (2) the longitudinal waves undergo a phase shift upon reflection, thereby complicating the calculation of the time of flight.

Table 7: Slopes of the wave speed vs. applied stress plots and the 95% confidence intervals obtained using the nonlinear least-squares method

Units: (m/s)/Pa	$\frac{\partial v_{22}}{\partial \sigma_{11}}$ (Fig. 5d)	$\frac{\partial v_{21}}{\partial \sigma_{11}}$ (Fig. 5e)	$\frac{\partial v_{23}}{\partial \sigma_{11}}$ (Fig. 5f)	$\frac{\partial c_R}{\partial \sigma_{11}}$ Hughes et al. [38]
Best fit	3.562e-8	-9.009e-8	3.706e-8	-3.534e-8
Lower 95% CI	3.211e-8	-9.132e-8	3.604e-8	-3.184e-8
Upper 95% CI	3.912e-8	-8.886e-8	3.809e-8	-3.884e-8

In addition to the measurement presented in Fig. 5, the absolute values of the bulk and Rayleigh wave speeds were also measured in the stress-free or unloaded configuration. The transverse wave speeds polarised in the mutually orthogonal e_1 and e_3 directions (see Fig. 4) were calculated to be v_{21} = 3069 m/s and v_{23} = 3101 m/s in the unloaded specimen, i.e. a difference of 32 m/s was observed. The speed of Rayleigh wave propagating in the unloaded specimen along the e_1 and e_3 directions were obtained as c_{R1} = 2812 m/s and c_{R3} = 2836 m/s, respectively. The latter speeds differed by 24 m/s. These differences indicate the directional dependence of wave speed, i.e. anisotropy of the unloaded specimen.

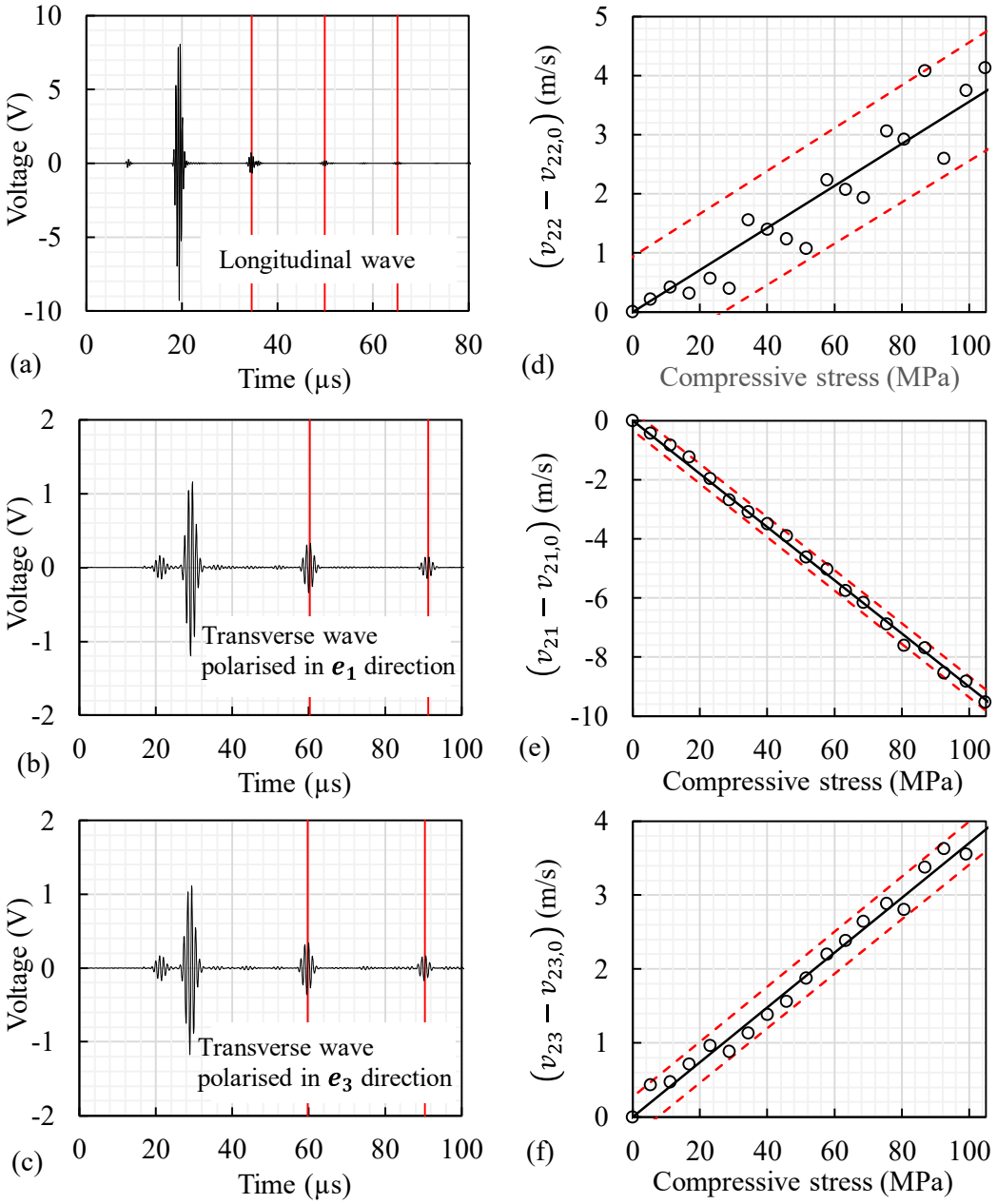

Fig. 5: (a)-(c) Time domain signal for three bulk waves propagating perpendicular to the applied stress recorded using a pair of ultrasonic transducers in pitch-catch arrangement. (d)-(f): Change in wave speed with incremental compressive loading – the circles represent the experimentally measured values, the solid lines represent the lines of best fit, and the broken lines represent 95% prediction intervals.

The TOECs can be determined from the experimentally measured slopes (Table 7) by using any three out of four linearised Eqs. (14)-(16), (B1). In accordance with the outcomes of

the validation test, which are summarised in Table 6, Method 4, i.e. the combination of Eqs. (15),(16) and (B1) is not used for the determination of the TOECs. The values of the TOECs calculated based on the remaining three methods are presented in Table 8. The values determined using all three methods lie within the broad range of previously published values for Aluminium alloys, some of which are summarised in Table 1. However, the values of the TOECs obtained using the three methods are not consistent with one another and the largest deviation is observed for the constant l.

The agreement between TOECs values using the three methods when using experimental data is not as good when compared against the outcomes of numerical study presented in Section 3, as well as the outcomes of the validation test of the linearised system of equations presented in Table 6. The discrepancies are attributed to the anisotropy of the tested specimen, which was ascertained from the unequal transverse wave speeds v_{21} and v_{23} in the unloaded specimen, as well as the unequal Rayleigh wave speed, c_{R1} and c_{R3} propagating along two mutually orthogonal directions. The difference in wave speed in the unloaded specimen was found to be 32 m/s for transverse waves polarised in orthogonal directions and 24 m/s of Rayleigh waves propagating in orthogonal directions. This initial difference, attributed to specimen anisotropy is significantly greater than the change in wave speed due to the acoustoelastic effect, as reported in Fig. 5 and Table 7. Hence, it may be argued that the erroneous results are due to the substitution of experimental data obtained for an anisotropic specimen into the equations of acoustoelasticity theory derived for isotropic materials. A better correspondence between the three methods for the experimental determination of TOECs can be achieved by taking into account the specimen anisotropy.

It is well known that the values of the TOECs can be affected by the changes in microstructure and accumulation of plastic deformations, which are expected to be quite

significant near the surface of the test specimen due to the fabrication process. Therefore, the obtained values can be interpreted as different parameters, which are related to the mechanical properties of an anisotropic and non-homogeneous material.

Table 8: TOECs determined from experimental measurements of bulk and Rayleigh wave speeds

TOEC	Mean (GPa)		
	Method 1 v_{22}, v_{21}, v_{23}	Method 2 v_{22}, v_{21}, c_R	Method 3 v_{22}, v_{23}, c_R
l	-193.2	-106.1	-249.5
m	-264.9	-222.4	-292.4
n	-333.4	-416.4	-351.4

6. Conclusion

In this paper, a new method for the evaluation of TOECs is presented. This method utilises measurements of the change in Rayleigh and bulk wave speeds with an applied stress. This method is applicable to homogeneous isotropic materials only as the theoretical equations are based on the same underlying assumptions. It was demonstrated via numerical simulations that the incorporation of Rayleigh wave speed measurements allows for a significant improvement in the accuracy of the evaluation of TOECs. While it is also theoretically possible to determine the TOECs solely from measurements of the Rayleigh wave speed due to the inherent non-linearity of the characteristic equation, such an evaluation requires highly accurate measurements as the non-linearity is relatively small.

In practical situations, the near surface material properties of the tested samples or structures are often different to the bulk. The inhomogeneity, anisotropy, accumulation of plastic deformation and damage associated with fabrication processes can affect the measurements of the elastic wave speed. In this case, the evaluation of the TOECs using these

measurements does not seem to be appropriate, as the constants obtained do not represent the bulk material properties. However, the actual changes in the wave speed can still be utilised for stress measurement purposes or for the characterisation of near surface mechanical damage. In addition, the near surface propagation nature of Rayleigh waves can be utilised for measurements of the change in stress, material properties and damage with depth. However, it would be very difficult to separate all these effects from one another in practical situations.

Acknowledgements

This work was supported by the Australian Government Research Training Program Scholarship, and the Australian Research Council, project DP160102233.

References

[1] D. S. Hughes, J. L. Kelly, Second-order elastic deformation of solids, Phys. Rev. 92 (1953) 1145–1149, doi: 10.1103/PhysRev.92.1145

[2] T. Bateman, W. P. Mason, H. J. McSkimin, Third-order elastic moduli of Germanium, J. Appl. Phys. 32 (1961) 928-936, doi: 10.1063/1.1736135

[3] E. H. Bogardus, Third-order elastic constants of Ge, MgO, and fused SiO2, J. Appl. Phys. 26 (1965) 2504-2513, doi: 10.1063/1.1714520

[4] Y. Hiki, A. V. Granato, Anharmonicity in noble metals; Higher order elastic constants, Phys. Rev. 144 (1966) 411-419, doi: 10.1103/PhysRev.144.411

[5] P. W. Bridgman, The effect of pressure on the rigidity of steel and several varieties of glass, Proc. Am. Acad. Arts Sci. 63 (1929) 401-420, doi: 10.2307/20026225

[6] P. W. Bridgman, The effect of pressure on the rigidity of several metals, Proc. Am. Acad. Arts Sci. 64 (1929) 39-49, doi: 10.2307/20026251

[7] F. Birch, The effect of pressure on the modulus of rigidity of several metals and glasses, J. Appl. Phys. 8 (1937) 129-133, doi: 10.1063/1.1710264

[8] F. Birch, The effect of pressure upon the elastic parameters of isotropic solids, according to Murnaghan's theory of finite strain, J. Appl. Phys. 9 (1938) 279-288, doi: 10.1063/1.1710417

[9] F. Birch, Finite elastic strain of cubic crystals, Phys. Rev. 71 (1947) 809-824, doi: 10.1103/PhysRev.71.809

[10] F.D. Murnaghan, Finite deformations of an elastic solid, Am. J. Math. 59 (1937) 235–260, doi: 10.2307/2371405

[11] L. Brillouin, Sur les tensions de radiation, Ann. Phys. Ser. 10 (1925) 528–586, doi: 10.1051/anphys/192510040528

[12] M.A. Biot, The influence of initial stress on elastic waves, J. Appl. Phys. 11 (1940) 522–530, doi: 10.1063/1.1712807

[13] M.A. Biot, Mechanics of Incremental Deformations, John Wiley, New York, 1965.

[14] L.D. Landau, E.M. Lifshitz, Theory of Elasticity, Butterworth-Heinemann, Oxford, 1986.

[15] F.D. Murnaghan, Finite Deformation of an Elastic Solid, John Wiley & Sons, New York, 1951.

[16] R.A. Toupin, B. Bernstein, Sound waves in deformed perfectly elastic materials. Acoustoelastic effect, J. Acoust. Soc. Am. 33 (1961) 216–225, doi: 10.1121/1.1908623

[17] M. Hayes, R.S. Rivlin, Propagation of a plane wave in an isotropic elastic material subjected to pure homogeneous deformation, Arch. Ration. Mech. Anal. 8 (1961) 15–22, doi: 10.1007/BF00277427

[18] D.R. Bland, Nonlinear Dynamic Elasticity, Blaisdell, Waltham, MA, 1969.

[19] Y.H. Pao, W. Sachse, H. Fukuoka, Acoustoelasticity and ultrasonic measurements of residual stresses, in W.P. Mason, R. N. Thurston (Eds.), Physical Acoustics, Academic Press, New York, 1984, pp. 61–143.

[20] A.N. Guz, F.G. Makhort, The physical fundamentals of the ultrasonic non-destructive stress analysis of solids, Int. Appl. Mech. 36 (2000) 1119–1149, doi: 10.1023/A:1009442132064

[21] A. Hikata, B. B. Chick, C. Elbaum, Dislocation contribution to the second harmonic generation of ultrasonic waves, J. Appl. Phys. 36 (1965) 229–236, doi: 10.1063/1.1713881.

[22] J. K. Na, J. H. Cantrell, W. T. Yost, Linear and nonlinear ultrasonic properties of fatigued 410Cb stainless steel, in D. O. Thompson, D. E. Chimenti (Eds.), Review of Progress in Quantitative Nondestructive Evaluation. Springer, Boston, 1996, pp. 1347–1351

[23] J. H. Cantrell, W. T. Yost, Acoustic harmonic generation from fatigue-induced dislocation dipoles, Philos. Mag. A, 69 (1994) 315-326, doi: 10.1080/01418619408244346

[24] K. Y. Jhang, Nonlinear ultrasonic techniques for nondestructive assessment of micro damage in material: A review, Int. J. Precis. Eng. Manuf. 10 (2009) 123-135, doi: 10.1007/s12541-009-0019-y

[25] K. H. Matlack, J. Y. Jacobs, L.J. Jacobs, J. Qu, Review of Second Harmonic Generation Measurement Techniques for Material State Determination in Metals, J Nondestruct Eval 34 (2015) 1-23, doi: 10.1007/s10921-014-0273-5

[26] J. Y. Kim, L. Jacobs, J. Qu, Nonlinear Ultrasonic Techniques for Material Characterization, in T. Kundu (Eds.), Nonlinear Ultrasonic and Vibro-Acoustical Techniques for Nondestructive Evaluation. Springer, Cham, 2019, pp. 225-261

[27] V. Marcantonio, D. Monarca, A. Colantoni, M. Cecchini, Ultrasonic waves for materials evaluation in fatigue, thermal and corrosion damage: A review, Mech. Syst. Signal. Process. 120 (2019) 32-42, doi: 10.1016/j.ymssp.2018.10.012

[28] D. M. Egle, D. E. Bray, Measurement of acoustoelastic and third-order elastic constants for rail steel, J. Acoust. Soc. Am. 60 (1976) 741-744, doi: 10.1121/1.381146

[29] R. T. Smith, R. Stern, R. W. B. Stephens, Third-Order Elastic Moduli of Polycrystalline Metals from Ultrasonic Velocity Measurements, J. Acoust. Soc. Am. 40 (1966) 1002–1008, doi: 10.1121/1.1910179

[30] S. Takahashi, Measurement of third-order elastic constants and stress dependent coefficients for steels, Mech Adv Mater Mod Process 4 (2018) 1-7, doi: 10.1186/s40759-018-0035-7

[31] J. Rose, Ultrasonic Guided Waves in Solid Media, Cambridge University Press, Cambridge, 2014, doi: 10.1017/CBO9781107273610

[32] M. Mohabuth, A. Kotousov, C. T. Ng, Effect of uniaxial stress on the propagation of higher-order Lamb wave modes, Int. J. Nonlinear Mech. 86 (2016) 104-111, doi: 10.1016/j.ijnonlinmec.2016.08.006

[33] R.W. Ogden, Incremental statics and dynamics of pre-stressed elastic materials, in M. Destrade, G. Saccomandi (Eds.), Waves in Nonlinear Pre-Stressed Materials, Springer, Wien, 2007, pp. 1–26.

[34] R.W. Ogden, Non-Linear Elastic Deformations, Ellis Horwood, Chichester, 1984.

[35] M. Destrade, R.W. Ogden, On stress-dependent elastic moduli and wave speeds, IMA J. Appl. Math. 78 (2012) 965–997.

[36] Z. Abiza, M. Destrade, R. W. Ogden, Large acoustoelastic effect, Wave Motion 49 (2012) 364-374, doi: 10.1016/j.wavemoti.2011.12.002

[37] M. A. Dowaikh, R. W. Ogden, On surface waves and deformations in a compressible elastic half-space, Stability Appl. Cont. Mech, 1 (1991) 27-45

[38] J. M. Hughes, J. Howie, J. Vidler, M. Mohabuth. Stress monitoring using the change in velocity of Rayleigh waves. In the proceedings of the 9th Australasian Congress on Applied Mechanics (ACAM9), 27-29 November 2017, Sydney, Australia.

[39] E. V. Nolde, L. A. Prikazchikova, G. A. Rogerson, Dispersion of small amplitude waves in a pre-stressed, compressible elastic plate, J. Elast. 75 (2004) 1–29, doi: 10.1023/B:ELAS.0000039920.67766.d3

Appendix A: Lamb wave dispersion equations

In this section, the derivation of the dispersion equations governing the acoustoelastic effect for Lamb waves is briefly recapped. The results presented in this Appendix were obtained previously in [32,39] and are included here for the sake of completeness. Consider an infinite, isotropic plate of thickness D, with the reference Cartesian coordinates X_1 and X_3 aligned with the mid-plane of the plate and the coordinate X_2 aligned with the outward normal from the mid-plane. The plate is subjected to a uniaxial stress state, with Cauchy stress σ_{11} along the X_1 axis. The finite deformation can be expressed as

$$x_i = \lambda_i X_i, \quad i \in \{1, 2, 3\}, \tag{A1}$$

where the principal stretches $\lambda_i = 1 + E_{ii}$ can be written in terms of the applied stress σ_{11} using Eq. (5). Now, consider the propagation of a small-amplitude plane wave confined to the $x_1 - x_2$ plane, travelling with phase velocity c in the x_1 direction. The general solution to the governing equation for incremental motions, Eq. (1), is of the form:

$$u_j = U_j e^{\xi \alpha x_2} e^{i\xi(x_1 - ct)}, \quad j = 1, 2, \tag{A2}$$

where u_j is the particle displacement and U_j is the amplitude along the x_j coordinate, ξ is the wavenumber along the x_1 direction, t is time and α is the unknown ratio of the wavenumbers in the x_2 and x_1 directions. The solution must satisfy the incremental traction-free boundary conditions at the upper and lower surfaces of the plate, i.e. the corresponding incremental nominal stresses must be zero at the free surfaces:

$$\hat{S}_{22} = \hat{S}_{21} = 0, \quad x_2 = \pm\frac{\lambda_2 D}{2} = \pm\frac{d}{2}. \tag{A3}$$

After substituting Eq. (A2) into Eq. (1), a system of linear homogeneous equations is obtained. Following the procedure outlined in Mohabuth et al. [32], the requirement for obtaining a non-trivial solution to this system of equations can be expressed as:

$$\begin{aligned} &\mathcal{A}_{2121}\mathcal{A}_{2222}\alpha^4 \\ &\quad + \{\rho c^2(\mathcal{A}_{2121} + \mathcal{A}_{2222}) - \mathcal{A}_{1111}\mathcal{A}_{2222} - \mathcal{A}_{1212}\mathcal{A}_{2121} \\ &\quad + (\mathcal{A}_{1122} + \mathcal{A}_{2121})^2\}\alpha^2 + \rho^2 c^4 - \rho c^2(\mathcal{A}_{1111} + \mathcal{A}_{1212}) \\ &\quad + \mathcal{A}_{1111}\mathcal{A}_{1212} = 0, \end{aligned} \tag{A4}$$

The lack of odd powers in the fourth-order Eq. (A4) implies that the four roots for α, denoted by $\alpha_q, q \in \{1, 2, 3, 4\}$ are related according to $\alpha_2 = -\alpha_1$ and $\alpha_4 = -\alpha_3$. Using this relation and the identity $e^z = \cosh(z) + \sinh(z)$, the solutions for u_1 and u_2 in Eq. (A2) can be

rewritten as a linear combination of the four independent solutions associated with the roots of Eq. (A4) as follows [39]:

$$u_1 = \{A_1 \cosh(\xi\alpha_1 x_2) + A_2 \sinh(\xi\alpha_1 x_2) + A_3 \cosh(\xi\alpha_3 x_2) + A_4 \sinh(\xi\alpha_3 x_2)\} e^{i\xi(x_1 - ct)},$$

$$u_2 = \left\{ \left(\frac{\mathcal{A}_{1111} - \rho c^2 - \mathcal{A}_{2121}\alpha_1^2}{i\alpha_1(\mathcal{A}_{1122} + \mathcal{A}_{2121})} \right) [A_1 \cosh(\xi\alpha_1 x_2) + A_2 \sinh(\xi\alpha_1 x_2)] + \left(\frac{\mathcal{A}_{1111} - \rho c^2 - \mathcal{A}_{2121}\alpha_3^2}{i\alpha_3(\mathcal{A}_{1122} + \mathcal{A}_{2121})} \right) [A_3 \cosh(\xi\alpha_3 x_2) + A_4 \sinh(\xi\alpha_3 x_2)] \right\} e^{i\xi(x_1 - ct)}, \quad \text{(A5)}$$

where the constants $A_q, q \in \{1, 2, 3, 4\}$ are functions of the displacement amplitudes $U_1(\alpha_q)$ in Eq. (A2).

The incremental stress components corresponding to (A5) can be obtained from the incremental stress-displacement relations given by Eq. (2). Satisfying the boundary conditions (A3) with the obtained incremental stress components yields a homogenous system of four equations in four unknowns, A_q. Using the method presented in Mohabuth et al. [32], two characteristic equations which ensure non-trivial solutions to this system of equations are obtained as:

$$\alpha_1(\eta - \zeta\alpha_3^2)\tanh(\gamma\alpha_1) - \alpha_3(\eta - \zeta\alpha_1^2)\tanh(\gamma\alpha_3) = 0, \quad \text{(A6)}$$

$$\alpha_1(\eta - \zeta\alpha_3^2)\tanh(\gamma\alpha_3) - \alpha_3(\eta - \zeta\alpha_1^2)\tanh(\gamma\alpha_1) = 0, \quad \text{(A7)}$$

which correspond to the anti-symmetric and symmetric Lamb wave modes, respectively, with $\gamma = \xi d/2 = \omega d/2c$. The constants η and ζ are defined as [39]

$$\eta = (\mathcal{A}_{1111} - \rho c^2)(\mathcal{A}_{1212} - \mathcal{A}_{2121} - \rho c^2),$$
$$\zeta = \mathcal{A}_{2222}\left(\mathcal{A}_{1111} - \frac{\mathcal{A}_{1122}^2}{\mathcal{A}_{2222}} - \rho c^2\right). \tag{A8}$$

The characteristic equation governing the acoustoelastic effect for Rayleigh waves propagating in an infinite half-space can be obtained by setting $\gamma = \xi d/2 \to \infty$ in equation (A6) or (A7) and recalling that $\lim_{\gamma\to\infty} \tanh(\gamma) = 1$, as follows

$$\eta + \zeta\alpha_1\alpha_3 = 0. \tag{A9}$$

Since Eq. (A4) is quadratic in α^2, the product $\alpha_1\alpha_3$ can be readily expressed as

$$\alpha_1\alpha_3 = \left(\frac{(\mathcal{A}_{1111} - \rho c^2)(\mathcal{A}_{1212} - \rho c^2)}{\mathcal{A}_{2222}\mathcal{A}_{2121}}\right)^{\frac{1}{2}}. \tag{A10}$$

Appendix B: Linearised Rayleigh wave characteristic equation

The characteristic Eq. (12) governing the propagation of Rayleigh waves along the direction of the applied uniaxial stress can be linearised for $\sigma_{11} \to 0$ as follows:

$$\mathcal{L}_1 + \mathcal{L}_2\mathcal{L}_3 + \mathcal{L}_4(\mathcal{L}_5 + \mathcal{L}_6) = 0, \tag{B1}$$

where the terms

$$\mathcal{L}_1 = -\left(C_{1111} - 2\rho_0 c_{R,0}\frac{\partial c_R}{\partial\sigma}\right)\rho_0 c_{R,0}^2 + \left(C_{1212} - C_{2121} - 2\rho_0 c_{R,0}\frac{\partial c_R}{\partial\sigma}\right)(\lambda + 2\mu - \rho_0 c_{R,0}^2), \tag{B2}$$

$$\mathcal{L}_2 = \left(\frac{\left(\lambda + 2\mu - \rho_0 c_{R,0}^2\right)\left(\mu - \rho_0 c_{R,0}^2\right)}{\mu(\lambda + 2\mu)}\right)^{\frac{1}{2}}, \tag{B3}$$

$$\mathcal{L}_3 = C_{2222}\left(\lambda + 2\mu - \rho_0 c_{R,0}^2\right) + \left(C_{1111} - 2\rho_0 c_{R,0}\frac{\partial c_R}{\partial \sigma}\right)(\lambda + 2\mu), \tag{B4}$$

$$\mathcal{L}_4 = (\lambda + 2\mu)\left(\lambda + 2\mu - \rho_0 c_{R,0}^2\right) - \lambda^2, \tag{B5}$$

$$\mathcal{L}_5 = \frac{\left(C_{1111} - 2\rho_0 c_{R,0}\frac{\partial c_R}{\partial \sigma}\right)\left(\mu - \rho_0 c_{R,0}^2\right) + \left(C_{1212} - 2\rho_0 c_{R,0}\frac{\partial c_R}{\partial \sigma}\right)\left(\lambda + 2\mu - \rho_0 c_{R,0}^2\right)}{2\left(\lambda + 2\mu - \rho_0 c_{R,0}^2\right)\left(\mu - \rho_0 c_{R,0}^2\right)}, \tag{B6}$$

$$\mathcal{L}_6 = -\left(\frac{C_{2222}\mu + C_{2121}(\lambda + 2\mu)}{2\mu(\lambda + 2\mu)}\right). \tag{B7}$$

In Eqs. (B2)-(B6), $c_{R,0}$ is the Rayleigh wave speed in the unstressed configuration, which can be determined in terms of the known material constants, λ, μ and ρ_0, by setting $J\mathcal{A}_{1111} = J\mathcal{A}_{2222} = (\lambda + 2\mu)$, $J\mathcal{A}_{1122} = \lambda$, and $J\mathcal{A}_{1212} = J\mathcal{A}_{2121} = \mu$ in Eq. (12). The dimensionless constants C_{ijkl} are closely related to the stress-dependent elastic moduli $\mathcal{A}_{ijkl}$, and are defined as follows:

$$C_{1111} = \frac{1}{3K}\left[2l + \lambda + \frac{\lambda + \mu}{\mu}(4m + 4\lambda + 10\mu)\right], \tag{B8}$$

$$C_{1212} = \frac{1}{3K}\left[m + \frac{\lambda}{4\mu}n + 4\lambda + 4\mu\right], \tag{B9}$$

$$C_{2222} = \frac{1}{3K}\left[2l - \frac{2\lambda}{\mu}(m + \lambda + 2\mu)\right], \tag{B10}$$

$$C_{2121} = \frac{1}{3K}\left[m + \frac{\lambda}{4\mu}n + \lambda + 2\mu\right], \tag{B11}$$

$$C_{1122} = \frac{1}{6K\mu}[4\mu l + 2\lambda m - \lambda n + 2\lambda(\lambda + 2\mu)]. \quad \text{(B12)}$$